Comparative study of different Sn wetted W CPSs exposed to NBI fluxes in the OLMAT facility

Fusion Engineering and Design 190 (2023) 113711

Contents lists available at ScienceDirect

Fusion Engineering and Design

journal homepage: www.elsevier.com/locate/fusengdes

Comparative study of different Sn wetted W CPSs exposed to NBI fluxes in the OLMAT facility

E. Oyarzabal [a,*], F.L. Tabarés [a], M. Liniers [a], D. Alegre [a], D. Tafalla [a], K.J. McCarthy [a], A. de Castro [a], T.W. Morgan [b], J.G.A. Scholte [b,c], M. Iafrati [d], E. de la Cal [a], I. Voldimer [a], E. Ascasíbar [a], A. Soleto [a], the OLMAT team [#]

[a] Laboratorio Nacional de Fusion, Av. Complutense, 40, Madrid 28040, Spain
[b] DIFFER—Dutch Institute for Fundamental Energy Research, De Zaale 20, Eindhoven, AJ 5612, the Netherlands
[c] Eindhoven University of Technology, Department of Applied Physics and Science Education, Groene Loper 19, Eindhoven, AP 5612, the Netherlands
[d] ENEA, Fusion and Nuclear Safety Department, C. R. Frascati, Via E. Fermi 45, Frascati (Roma) 00044, Italy

ARTICLE INFO

Keywords:
Capillary porous systems
Liquid metals
High heat flux facilities
DEMO divertor
Plasma wall interaction
Neutral beam injector

ABSTRACT

Four different tin-wetted, tungsten CPS (Capillary Porous System) targets where exposed to NBI pulses in the OLMAT High Heat flux (HHF) facility. They include two flexible ones placed on a TZM support (W meshes and W felt) and two compact ones (sintered W disk and 3D printed W). A comparative study was performed using a fast-frame imaging camera and an infrared pyrometer. Surface temperature increase and homogeneity, particle ejection, CPS damage and overall behaviour were studied for each case. Sn drop/accumulation at the lower part of the targets was observed for all cases when they are heated up to around 400 °C except for the 3D printed W target that has its own Sn deposit. The 3D printed W target presented the best results in all aspects, withstanding heat pulses up to 58 MW/m^2 in 100 ms without any damage or particle ejection. On the other hand, the W mesh targets displayed damage at 20 MW/m^2 due to a bad thermal contact with the deposit, while the sintered W disk developed a crack during a series of 15 MW/m^2 NBI pulses. As might be expected, a reduced increase of temperature during pulses is observed for the two compact W targets. The results and their relevance for the design of a Sn wetted W CPS for application as a DEMO-divertor material are discussed in the present work.

1. Introduction

The application of liquid metals (LM) as plasma facing materials has been considered a potential solution for the technical issues associated with power exhausting and particle handling in magnetic confinement fusion devices at the reactor level. Extensive research has been performed in the past showing liquid metals (LMs) as a promising candidate for plasma facing material [1–4]. Their most interesting advantages are the self-healing/renewability of the plasma-facing surface and their lower sensitivity to neutron damage. As a result, increased lifetime with respect to that of a solid wall is expected. Pre-conceptual design activities performed under the auspices of EuroFusion have identified Sn as the leading candidate as a liquid metal and CPSs as the most mature technology option for implementation in EU-DEMO. The main reasons for selecting Sn over lithium were its lower tritium retention, very similar to that of W, its the lower vapour pressure and the fact that exposure to atmosphere at room temperatures (maintenance) does not result in problematic oxidation, or safety hazards. Design activities for a possible Sn wetted CPS divertor for EU-DEMO have already started [5,6] and experiments exposing different Sn CPSs to heat fluxes and conditions similar to those of a divertor are of major importance in order to reach the optimal design and to find any possible issues in their future application as divertor materials. In this regard, the OLMAT HHF facility at CIEMAT, where the present work has been carried out, is mainly devoted to testing these types of liquid metal CPS components under High Heat fluxes.

The final choice of the porous structure in a CPS target must consider several factors, i.e., from both technological and physical points of view. These factors are sometimes contradictory and the final performance of the chosen CPS structure can be only experimentally tested in dedicated

* Corresponding author.
E-mail address: eider.oyarzabal@ciemat.es (E. Oyarzabal).
[#] The OLMAT Team: Ricardo Carrasco, Fernando Martin, Miguel Navarro, Andrés Jiménez-Denche, Francisco Miguel Honrubia, Luis Alberto Bueno, José A Sebastián, Emilio Sánchez, Ana Portas, Augusto, Pereira, Ángel de la Peña and Jesús Gómez.

https://doi.org/10.1016/j.fusengdes.2023.113711
Received 11 October 2022; Received in revised form 12 March 2023; Accepted 29 March 2023
Available online 3 April 2023

facilities. On the one hand, the flexibility, technical simplicity and easy replacement of mesh-type structures make them highly suited for the purpose, however, maintaining good thermal contact with the metallic substrate under high temperature, cyclic excursions, is challenging and their destruction upon plasma exposure has been reported in previous tests [7]. On the other hand, more robust porous structures, such as those provided by sintered metals and 3D printed blocks, although less prone to deformation issues, also show some shortcomings. For instance, for sintered targets, with pore sizes in the sub-micron range, the slow transport of the liquid metal under these geometries may prevent the timely refilling of the exposed surface when exposed to the plasma, particularly if fast transients are involved in the interaction. Also, they may become fragile under the strong thermo-mechanical stresses arising under divertor operation. More recently, quite promising results have been obtained for the use of 3D-pinted structures as the porous component of a CPS target [7]. One of the main goals of this concept is the minimization of thermal stress at the relevant temperatures of reactor operation, while fast refilling of the surface is guaranteed by a combination of narrow channels at the surface (providing strong capillary forces) and large voids directly connected to them. In this work, we compare these different types of CPS targets with regards to surface temperature increase and homogeneity, particle ejection, CPS damage and overall behaviour using a fast-frame imaging camera (FASTCAM SA1 with a top speed in excess of 600,000 fps and with true 12-bit dynamic range) and an infrared (IR) pyrometer (OPTRIS CTlaser3MH1 with 2,3 μm spectral range and a temporal resolution of 1 μm) in order to obtain relevant information for the design of a liquid Sn CPS DEMO divertor. Finally, although the OLMAT facility is equipped with many other diagnostics [8,9], we focus on fast camera and pyrometer results in this study.

The paper is organized as follows. The experimental set-up, including a brief description of the OLMAT High Heat Flux Facility, is explained in Section 2. Section 3 is devoted to the description of the different CPS prototypes used in this study. The results, shorted by case study, are presented and discussed in Section 4, and a summary of them together with the conclusions is given in Section 5.

2. Experimental set-up

The experiments presented here were carried out in the OLMAT facility, which was described previously in detail [8,9], so only a sketch is shown in Fig. 1. One of the two neutral beam injectors (NBI) operated on the stellarator TJ-II is used to irradiate samples in a separate, diagnosed chamber of 60 × 60 × 40 cm^3 under high vacuum conditions. Thus, the Sn wetted W CPS with its target holder is installed on a manipulator with heating, biasing, translation, and rotation capabilities. In order to prevent overheating of the duct that connects the OLMAT chamber to the TJ-II vacuum vessel, two retractable molybdenum plates are inserted behind the manipulator. These plates have thermocouples incorporated into them, these being placed on the backside of the plate (unexposed to NBI) so that a shot-to-shot recording of their temperature can be made. Infrared pyrometry and IR thermography [8] allow the temperature evolution of the exposed surface to be followed with 1 ms time resolution. Both temperature sensors, as well as embedded thermocouples, are used to characterize the thermal response of the sample and to assess the incident heat flux. For each target, the infrared pyrometer is calibrated in the laboratory with a thermocouple up to 550 °C. There is a linear relation between the thermocouple temperature and the pyrometer voltage in this range, indicating a constant emissivity of the Sn surface up to 550 °C. For temperatures above 550 °C the same calibration is used so the possible emissivity changes at higher temperatures are not taken into account in the present work, experiments to extend this calibration up to 800 °C are underway.

During the commissioning phase of OLMAT the capabilities of the NBI where studied by exposing a TZM target to its beam. Heat fluxes for different NBI powers were calculated from calorimetry and an upper limit was obtained by assuming total thermal coupling between the TZM target and the stainless steel (SS) holding ring of its target holder while a lower limit was obtained by assuming no thermal coupling between them. Heat fluxes up to 58±14 MW/m^2 in 100 ms pulses and series of 100 pulses (100 ms duration) at 30 MW/m^2 were reached. Also a repetition rate of 2 pulses per minute and maximum pulse length of 150 ms was achieved at low/medium heat fluxes (below 30 MW/m2). The beam presents a gaussian profile of FWHM 11.7 cm for a heat flux of 15 MW/m^2. More details of these results are given in [9]. In this work, average values of the calculated heat fluxes for the NBI power are used.

A scheme of the target holder is shown in Fig. 2. It consists of a supporting SS plate (a), a TZM holding ring of 10 cm diameter (b), isolating ceramics (d) and a heating wire (e). In this set-up the target is electrically and thermally isolated from the supporting plate by the ceramics and it can be heated up to 700 °C via current in the heating wire. An 80 mm diameter and 7 mm thick TZM disc (c) was machined to produce an array of 2 mm diameter holes of 3 mm depth evenly distributed over its surface and separated by 10 mm. These holes are designed to act as LM reservoirs for CPS exposure experiments, while reducing the flexing of any material on top of it. This deposit is used for the case of the three W mesh CPS and the W felt CPS, whilst in the case of sintered W and 3D W targets special TZM masks were machined to accomplish the geometrical accommodation of the targets in the target holder (see next section for a complete description of the different targets). Finally, two thermocouples (f) are place at the bottom of the targets.

3. Sn filled CPS targets

Four different Sn wetted W CPS targets were studied for this work. The targets are seen in Fig. 3 and their main characteristics are summarized in table 1.

The first W CPS wetted target (a) is the only one that was designed

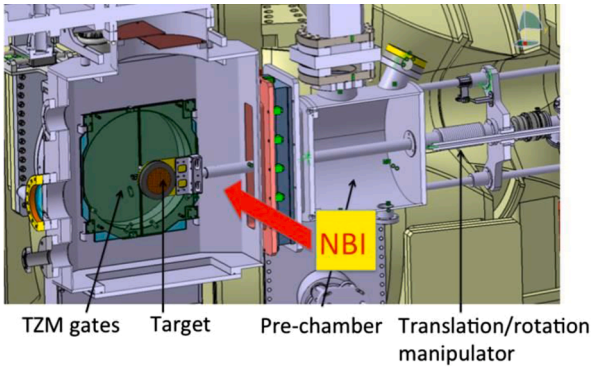

Fig. 1. Sketch of the OLMAT facility.

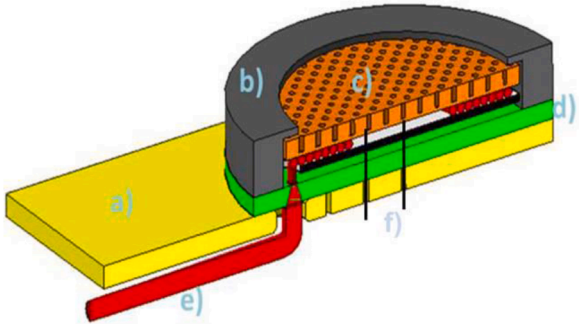

Fig. 2. OLMAT target holder scheme: supporting SS plate (a), holding TZM ring (b), liquid Sn TZM deposit (c), isolating ceramics (d), heating wire (e) and thermocouples (f).

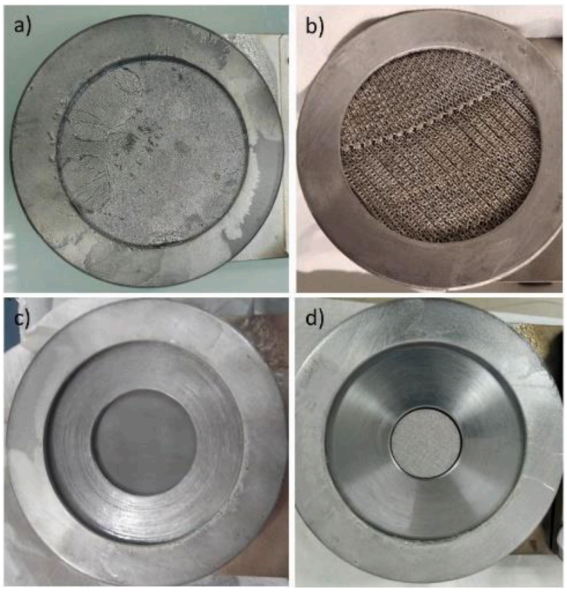

Fig. 3. Four Sn wetted W CPS targets exposed to OLMAT: W meshes (a), W felt (b), sintered W disk in the centre of the target (c) and 3D printed W in the centre of the target (d).

Table 1
Main characteristics of exposed Sn wetted W CPS.

	W meshes	W felt	Sintered W disk	3D printed W
Diameter of exposed area (mm)	70	70	37	25
Thickness (mm)	1	3	3	17
Pore size (μm)	50 effective/150 each mesh	500	>1	100

and manufactured by the Plasma-wall Laboratory at CIEMAT. It is the simplest design of the four designs used here. In this case, the TZM deposit described in the previous section acts as the primary substrate where a set of three porous W meshes (150 μm pore diameter each giving a 50 μm effective pore diameter) are placed on top of it and clamped together with the holding TZM ring. In this way, the liquid Sn spreads along the porous mesh and is confined therein by capillary forces.

The wetting of the target was performed for about 5 min in a vacuum oven that can reach 1150 °C. These high temperatures are needed for the wetting of W with Sn. However, several challenges were encountered to achieve a good wetting. The target was placed in the oven with several solid pieces of Sn placed on top of it (Fig. 4). In the first attempt only partial wetting was achieved because some Sn spilled onto the floor of the oven (circled in red). Two of the Sn pieces did wet the W mesh (upper part) but the rest where spilled through the side of the target when melted, forming the tin puddle that can be observed inside the red circle. In order to overcome this problem several pieces of W were placed between the holding ring and the lateral part of the liquid metal reservoir (element marked with c in Fig. 2) to avoid the spilling through this area. In this way, a more homogeneous wetting and distribution of liquid metal over the whole porous surface was achieved (Fig. 3a).

Nevertheless, there was some oxidation of Sn as the pressure in the vacuum oven reached about 200 mTorr during wetting. On the other hand, there was some bulging in the centre of the meshes, due to the heating process followed by thermal expansion of the clamped mesh, which led to poor contact of that area with the deposit and this became quite problematic when exposing the target to OLMAT. Two tungsten (W) wires were set across the CPS surface to prevent the bulging when exposed to the NBI in OLMAT, however this solution was ineffective.

Fig. 4. Second attempt at Sn wetting of the W meshes due to spilling of Sn (red circle) during the first wetting.

The second target (b) was manufactured at the ENEA institute. It consists of W wires which give it some flexibility, as in the case of the three meshes target, and allow it to conform more easily to different shapes than the other two more robust CPSs. This felt is also placed on top of the TZM deposit and they are clamped together with the holding TZM ring.

The third target (c) is a Sn wetted sintered W disk provided by the DIFFER institute that is exposed with a TZM masque on top of it in order to adapt it to the target holder, as can be seen in Fig. 3c. In this case, there is no TZM deposit (Fig. 2c) and the sintered W disk is fixed in place with a cup of TZM in its backside. This target presents a very small pore size (< 1 μm) and it was underfilled with Sn (only 30% of the porous volume) due to technical problems during wetting.

Finally, the forth target (d) is a 3D printed W target provided by the DIFFER institute. It incorporates its own deposit, so there is no TZM deposit (Fig. 2c) for this case either, and presents a series of internal channels that allow the Sn in the deposit to wet the porous surface by capillarity. A section is shown in Fig. 5. It is hold in place in the target with a TZM ring around it in the back of the TZM masque. This 3D printed W CPS was also used in the experiments performed in Magnum and reported in [7,7].

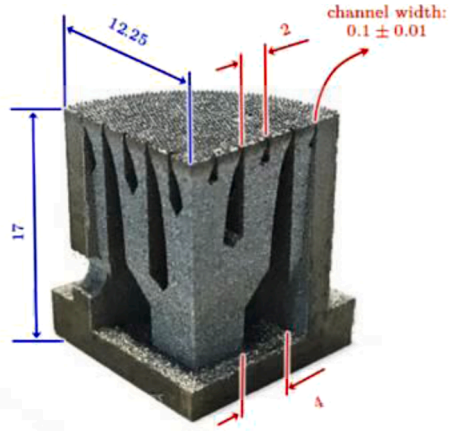

Fig. 5. Section of the 3D printed W target [10].

4. Results and discussion

In this section results related to target surface temperature increase and homogeneity, particle ejection, CPS damage and overall behaviour/performance of the four targets are shown and discussed. During the experiments, the targets were exposed to increasing heat fluxes and increasing pulse time (30–50–70–100 ms) for each heat flux. In the case of the W meshes and W felt targets, due to the high temperatures reached during the pulses and the problems associated with the evaporation of Sn the experiments where stopped at a maximum heat flux of 20 MW/m^2, for the case of the sintered W target a maximum heat flux of 50 MW/m^2 was reached and for the 3D printed W target the maximum allowable heat flux in OLMAT (58±14 MW/m^2) was reached during the experiments.

4.1. Drop formation/accumulation of Sn at bottom

In the test facility, the targets are set vertical, thus the term "bottom" used here refers to the lower part of the target. As can be observed in Fig. 6, Sn drop formation occured in the three W meshes targets (a) and in the sintered W disk (b) and Sn accumulation was observed at the bottom of the W felt target (c) as the surface temperature increased. Only the 3D printed W target, that had its own Sn deposit and had been exposed previously to MAGNUM [7] did not show this effect. Such behaviour for liquid Sn CPSs was previously reported in the experiments performed in [10]. For the W felt and Sintered W targets this was observed as the target was heated during exposure to the NBI pulses but in the case of the three W meshes this was also observed in the laboratory where some dedicated experiments were carried out.

In this case, the drop observed at the bottom appeared when the target was heated up to around 400 °C and was reabsorbed again during target cooling (Fig. 7), thus indicating a lower available volume within the folded mesh at higher temperatures. This effect could be related to the increase in volume of Sn with increasing temperature, to gravity and probably to a reduced thickness of the Sn wetted layer for higher Sn temperatures. Further experiments are necessary to fully address this issue as this is very relevant for designing a suitable Sn wetted W CPS for its application as a DEMO divertor.

4.2. Surface temperature inhomogeneity and droplet ejection

The surface temperature inhomegenity and droplet ejection was observed with a high-speed CMOS camera, Photron SA1 [11]. Inhomogeneities in the temperature increase and particle ejection can be observed due to blackbody emissions that are related to temperature. The camera is a black and white camera for which the brighter spots represent higher temperatures. Additionally, in some cases, a filter than transmits Sn lines was used on the camera to observe Sn evaporation.

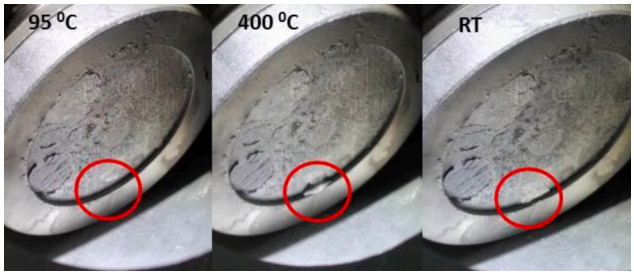

Fig. 7. Drop formation upon heating the Sn wetted W meshes target at 400 °C and reabsorption at RT.

a) Sn-wetted W meshes:

The Sn-wetted W mesh target presents large surface temperature inhomogeneities due to poor wetting and contact with the TZM deposit as has been explained before (as a consequence of the central bulging of the CPS structure). As can be observed in Fig. 8, the areas with poor thermal contact with the deposit reach higher temperatures (white areas) than the rest of the target. Droplet ejection was observed from these areas at heat fluxes of about 15 MW/m^2.

In addition, some displacement of Sn inside the target seems to have

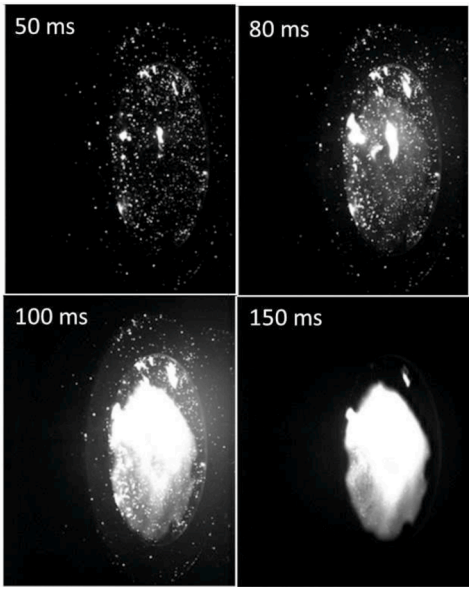

Fig. 8. Fast camera results for 15MW/m^2 and 100 ms pulse at 300 °C initial temperature. Formation of hot spots in the central region of the target is visible.

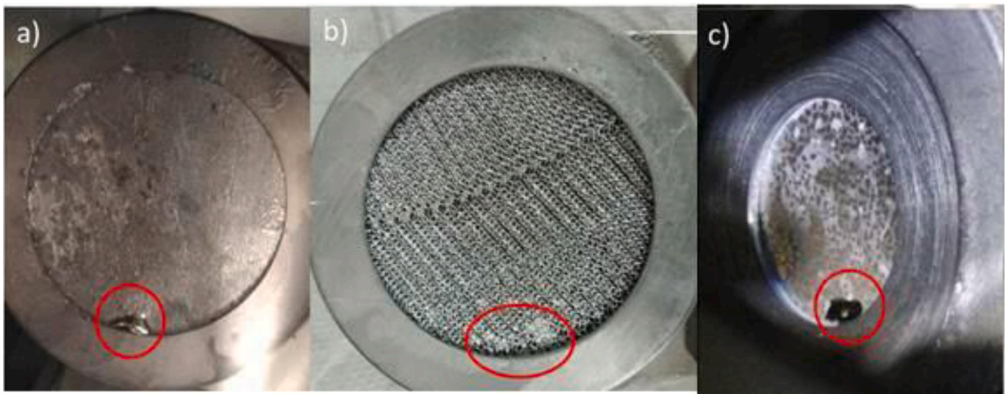

Fig. 6. Drop formation/accumulation of Sn (red circle) in all targets except for the 3D rpinted W.

taken place. On the one hand, the white spots of the target (that correspond to the highest temperatures) changed over the operational days, as can be observed in Fig. 9. Apart from the brighter part at the centre, which is related to the before mentioned bending of the meshes, there is a bright area in the upper left side that moves to the upper right side over the operational days. This observation points to liquid metal redistribution along the porous structure as a consequence of the evaporation-refilling cycle.

On the other hand, Fig. 10a shows a dried out area in the upper left side of the target (the deposit holes are visible within the red circle) when it is at 280 °C that gets filled with Sn when the target is cooled down (Fig. 10b). This indicates movement/redistribution of Sn inside the CPS-TZM deposit that possibly depends on temperature, wetting, gravity and amount of available Sn. It should be taken into account that there was significant evaporation in this target. Thus, at the end of the experiments, it may have experienced a depletion of Sn (dry out) when the deposit becomes empty.

a) Sn-wetted W felt:

In Fig. 11 it is seen that surface heating is more homogeneous during a pulse for this target than in the previous case except for the protuberance present in the target itself. In this case, there is no drop formation at the bottom. However, for temperatures around 400 °C there is a clear accumulation of Sn at the bottom which makes that area colder (darker) in comparison with the rest during the pulse (Fig. 11b).

In this target, we observe droplet ejection at about 10 MW/m^2 but only for the case of 280 °C initial temperature of the target. When the target was heated to an initial temperature of 460 °C no further droplet ejection was observed even up to 20 MW/m^2 heat fluxes. As the exposures at lower temperature (280 °C) were performed at the beginning of operation with the target, it appears that the target conditioning effect is responsible for the observed droplet ejection at this temperature. Experiments performed with this target in a more recent campaign have shown that after the target has been conditioned no particle ejection is observed even at 280 °C initial temperature.

a) Sn-wetted W sintered disk:

In Fig. 12, inhomogeneities were also observed in the case of the W sintered disk as its surface temperature increased during a pulse. In this case, a drop forms at the bottom of the target (red circle) even when the initial target temperature is 300 °C and the upper part of the target has a higher temperature than the rest of the target both during and after the pulse. This is probably due to a lack of Sn in the upper part due to an accumulation at the bottom. Once the pulse has finalized (at 170 ms), isle structures are also visible all over the target, pointing to dried out areas close to wetted areas. This is the only target that presents this kind of structures. It is considered here that is related to under filling of the target with Sn and to the very small pore size. Finally, some particle ejection was observed but only from the unbound Sn present in the bottom drop.

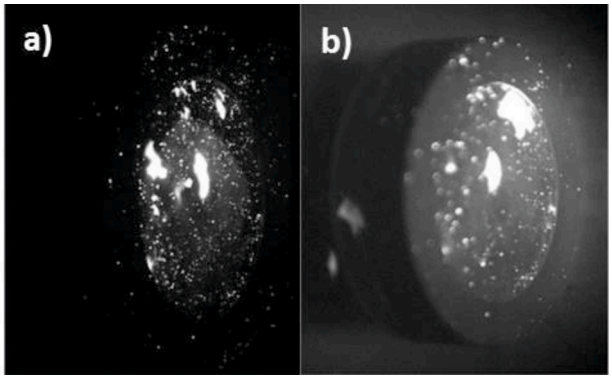

Fig. 9. Fast camera results for (a) 10MW/m^2 and 100 ms pulse (first day of operation with target) and (b) 8MW/m^2 and 50 ms pulse (last day of operation with target).

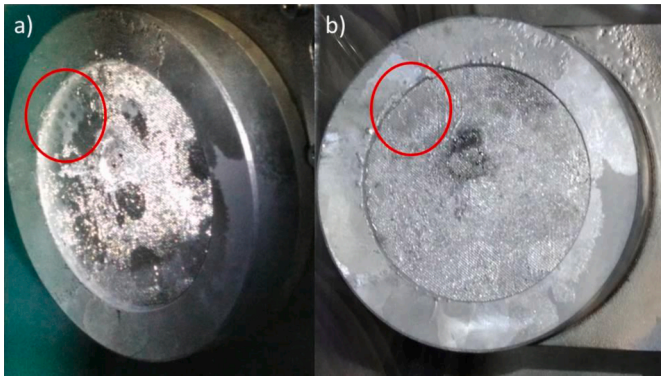

Fig. 10. (a) Dryed out area on the upper left side (red circle) at 280 °C and (b) same area filled with Sn (red circle) when the target is cooled down.

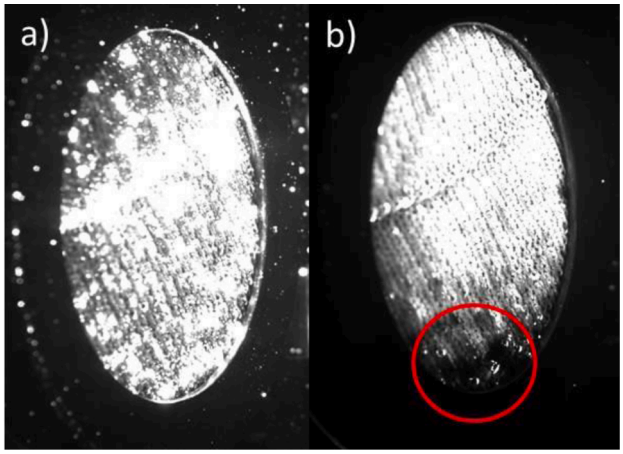

Fig. 11. Fast camera results for (a) a 80 ms 10 MW/m^2 pulse with 280 °C initial temperature and (b) a 100 ms 10 MW/m^2 pulse with 460 °C initial temperature.

Next, to study its fatigue behaviour, the target is exposed to a series of 50 pulses of 15 MW/m^2 heat flux and 150 ms duration every 150 s. In this case, a crack formed in the left side of the target after only five pulses. This area with the crack reached much higher temperatures than the rest of the target. This is identified as the bright area in left side region of the image after crack formation in Fig. 13. The additional heating of this area by the NBI beam can be related to the fact that the crack is formed by two sharp edges. Indeed, because of the high temperatures reached by the cracked area, Sn evaporation became a problem, and this complicated the completion of experiments and limited the achievable heat flux before viewport window metallization started. In some cases a dried out surface was also observed (visual observation) before the pulse, with Sn flowing to the surface as the pulse started. These observations reflect the paramount importance of achieving sufficient homogeneity in thermal behaviour and global performance over the liquid-metal CPS surface target.

a) Sn-wetted 3D printed W:

The 3D printed W target presented the best performance with respect to surface temperature increase homogeneity during the NBI pulses. As can be observed in Fig. 14, the hot spots (white spots) related to surface rugosity are homogenously distributed over the target during the whole

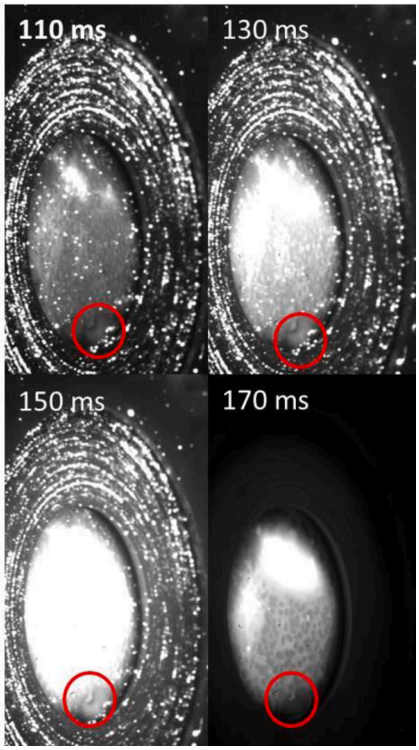

Fig. 12. Fast camera images for a 25 MW/m^2 and 150 ms pulse at 300 °C initial temperature. The image times along the pulse are shown. A Sn drop that occurs of the bottom of the target is highlighted by a red circle.

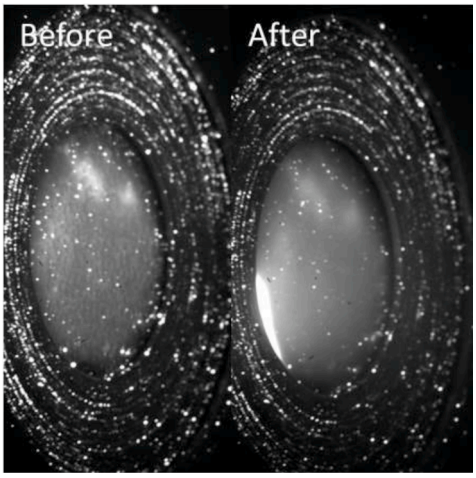

Fig. 13. Fast camera images before and after crack formation in the Sn-wetted W sintered disk target when testing with 15 MW/m^2 and 150 ms long NBI pulses.

pulse duration (110 ms). In addition, no differences are observed between the upper part and lower part after the pulse, as occurred in the previous cases. It seems that in this case, where the target has its own deposit and Sn is supplied to the surface by capillarity, no drop/accumulation of Sn occurs at the bottom of the target. Furthermore, no particle ejection was observed from this target at any time along the pulse even when rising to the highest allowable heat fluxes at OLMAT, i.e., 58± 14 MW/m^2.

On the other hand, heat fluxes of the order of 44±10 MW/m^2 and 100 ms pulse lengths were needed to achieve a sufficiently high temperature (around 1100 °C) to observe a visible evaporative cloud above this target. The images in Fig. 15 show the evolution of this evaporative

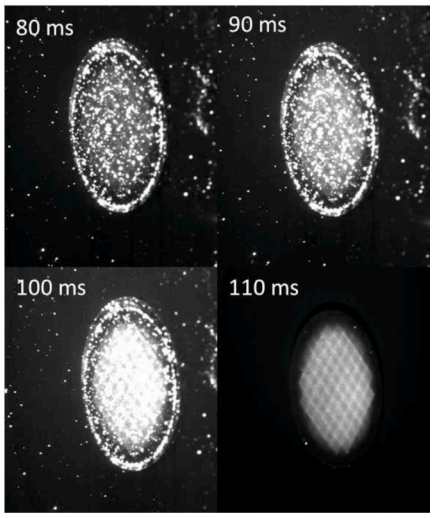

Fig. 14. Fast camera images for the Sn-wetted 3D printed W target, with a 280 °C initial temperature, for a 100 ms pulse with 30 MW/m^2 heat flux.

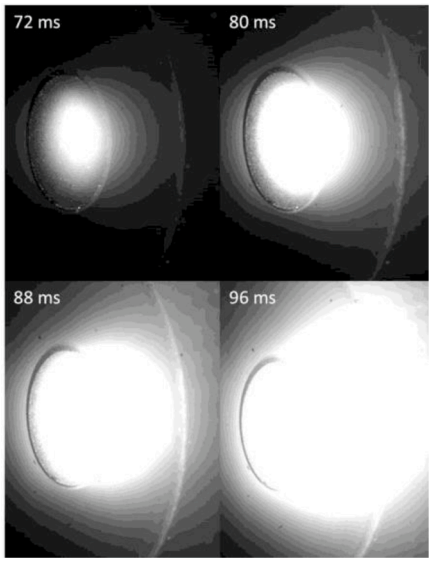

Fig. 15. Fast camera images with sn filter recorded for a 44 MW/m^2 and 100 ms long pulse for a Sn-wetted 3D printed W target with an initial temperature of 280 °C.

cloud. These images were recorded using a Sn filter fitted to the camera for a 44±10 MW/m^2 and 100 ms long pulse with an initial target temperature of 280 °C. As occurred with temperature, a very homogeneous evaporation is observed for this target.

4.3. Surface temperature increase during a pulse

With regard to target surface temperature increase during a NBI pulses there exists a clear difference between the W mesh and W felt targets and the other two more compact targets. The first two behave in a similar manner, reaching values of almost 1100 °C at 15 MW/m^2 and 100 ms pulse lengths with a mean temperature increment of about 9 °C/ms. This temperature is rather high and it is probably related to poor thermal contact between the meshes and felt and the deposit. On the other hand, the sintered W and 3D printed targets present similar temperature increments, reaching about 650 °C for a 15 MW/m^2 and 100 ms long pulse with a mean temperature increment of about 3.5 °C/ms. See Fig. 16. For these latter targets, the heat flux has to be increased up to

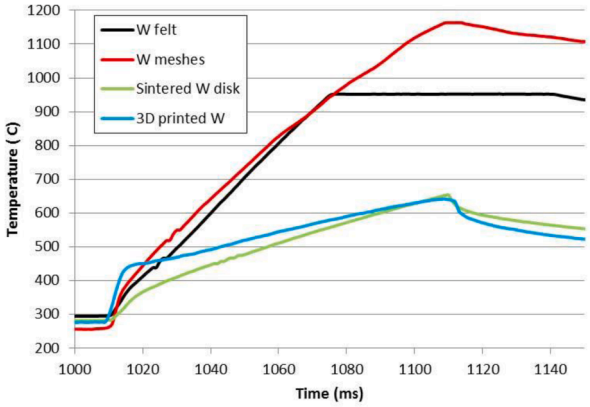

Fig. 16. Comparison of the temperature increment measured by the pyrometer for the four different Sn wetted W CPS subjected to a 100 ms long pulse producing 15 MW/m^2 on a target with 280 °C initial temperature (in the W felt case the pyrometer saturates at 1075 ms).

values of 44±10 MW/m^2 during a 100 ms pulse in order to reach temperatures close to 1100 °C.

An interesting effect is observed in the case of the Sn-wetted W felt target; when increasing the initial temperature of the target the temperature increment during the pulse becomes lower (see Fig. 17). This could be related to a better contact with the deposit for higher temperatures of Sn or to a change in the CPS thermal properties with temperature. Simulations of the temperature increase of the targets are underway and may give some insight about these results.

4.4. CPS damage

No damage was observed in the W felt target for incident heat fluxes up to 20 MW/m^2. However, due to the high evaporation occurring for these heat fluxes, it was not possible to achieve higher heat fluxes with this target. Also, the 3D printed target did not show any sign of damage either up to 58 MW/m^2 heat fluxes, the maximum reachable heat flux with the NBI at OLMAT.

In contrast, the W mesh and W sintered targets did show some damage. As can be seen on the left of Fig. 18, the upper most W mesh of the three mesh W target shown here presents a hole in the central part after a 20 MW/m^2 and 100 ms pulse. This is the area where the meshes were bent and thus had no contact with the liquid-Sn deposit

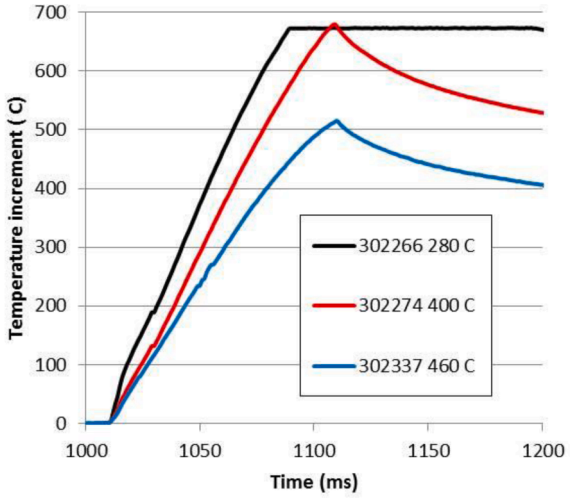

Fig. 17. Comparison of temperature increment during 10 MW/m^2 and 100 ms long pulses when increasing the initial temperature of the W felt target (the pyrometer saturates at around 1075 ms for pulse #302,266).

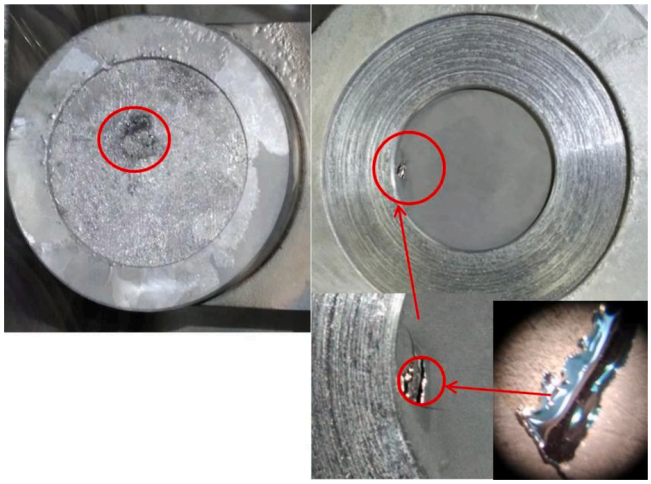

Fig. 18. Damages observed in the three W meshes target and the Sintered W disk target.

underneath. The fact that this mesh presents a hole suggests that the temperature reached during the pulse was high enough to melt the W mesh (probably reaching more 3000 °C). It also shows that the Sn in the surrounding area was unable to refill that part of the mesh as Sn was evaporated from it during the pulse. This may be due to a lack of Sn in the target at the end of the experiments since significant Sn evaporation had already taken place. This is also in agreement with the lack of Sn observed in Fig. 10.

In addition, as mentioned previously, the sintered W target presented some damage after about 5 pulses of 15 MW/m^2 heat flux and 150 ms pulse durations with a 150 s interval between pulses. In this case, a crack forms on the left side of the target as seen in the right side image of Fig. 18. Although the reason for the formation of the crack is unclear, we consider that it could be due to the presence, before exposure, of a small defect in that area of the sintered W disk and to the fact that there is a small clearance between the sintered W disk and the TZM masque that allows very small relative movements during a beam pulse. Due to the high temperature reached in the cracked area, evaporation of Sn became a problem for the rest of the experiments and limited the achievable heat flux before window metallization started. Nevertheless no more damage in the rest of the target was observed for pulses up to 50 MW/m^2 and 100 ms long.

Summary and conclusions

Four different Sn-wetted W CPS targets were exposed to NBI pulses in the OLMAT facility. A comparative study of surface temperature increase and homogeneity, particle ejection, CPS damage and overall behaviour has been performed using a fast-frame imaging camera and an IR pyrometer. From this comparative study, the following conclusions can be considered for the design of a future Sn-wetted W CPS for application as a DEMO divertor material:

- Good wetting and good contact with the structure in which the CPS is placed is very important in order to achieve good thermal conductivity and avoid inhomogeneities in the CPS surface temperature and concomitant formation of hot spots and associated dried-out areas for the meshes approach case. If this cannot be achieved, then this type of CPS is not recommended. In this sense, the W felt target, which keeps the flexibility advantage of this kind of CPS, presents better behaviour.
- It has been observed that Sn tends to form a drop at the bottom of targets when the target temperature increases to values around 400 °C during a pulse or when simply externally heated. This phenomenology could be related to the interplay of gravity forces with

capillary ones and to changes in this balance that might be associated with variations in the fluid characteristics of tin with increasing temperature. Furthermore, particle ejection is observed from the drop, this probably being due to splashing. This can only be avoided in the case of the 3D printed W target, which has its own Sn deposit. Designs with characteristics similar to the 3D printed W target are therefore encouraged.

- The reduced pore size causes problems such as isle formation and drying out of the Sn-wetted sintered W target surface in certain cases and should be avoided.
- Small defects in the sintered W disks can result in crack formation with exposure. Higher evaporation from the cracked area is observed when compared with the rest of the undamaged target. This could represent a serious problem if used as a divertor material.
- As could be expected, lower temperature increments are observed during pulses for more compact targets. In this regard experiments with more compact W felts from ENEA are planned in order to see its effect on surface temperature increase.
- The 3D printed W target shows the best results with no damage or droplet ejection up to 58 MW/m^2.

Declaration of Competing Interest

The authors declare that they have no known competing financial interests or personal relationships that could have appeared to influence the work reported in this paper.

Data availability

Data will be made available on request.

Acknowledgments

This work has been carried out within the framework of the EUROfusion Consortium, funded by the European Union via the Euratom Research and Training Programme (Grant Agreement No 101052200 - EUROfusion). Views and opinions expressed are however those of the author(s) only and do not necessarily reflect those of the European Union or the European Commission. Neither the European Union nor the European Commission can be held responsible for them.

References

[1] F.L. Tabarés, Present status of liquid metal research for a fusion reactor, Plasma Phys. Control. Fusion 58 (2015), 014014.
[2] R.E. Nygren, F.L. Tabarés, Liquid surfaces for fusion plasma facing components—a critical review. Part I: physics and PSI, Nucl. Mater. Energy 9 (2016) 6.
[3] A. de Castro, et al., Lithium, a path to make fusion energy affordable, Phys. Plasmas 28 (2021), 050901.
[4] T.W. Morgan, et al., Liquid metals as a divertor plasma-facing material explored using the Pilot-PSI and magnum-PSI linear devices, Plasma Phys. Control. Fusion 60 (2018), 014025.
[5] S. Roccella, G. Dose, R. de Luca, M. Iafrati, A. Mancini, G. Mazzitelli, CPS Based liquid metal divertor target for EU-DEMO, J. Fusion Energy 39 (2020) 462.
[6] P. Rindt, et al., Conceptual design of a liquid-metal divertor for the European DEMO, Fusion Eng. Des. 173 (2021), 112812.
[7] P. Rindt, et al., Using 3D-printed tungsten to optimize liquid metal divertor targets for flow and thermal stresses, Nucl. Fusion 59 (2019), 054001.
[8] D. Alegre, et al., Design and testing of advanced liquid metal targets for DEMO divertor: the OLMAT project, J. Fusion Energy 39 (2020) 411.
[9] F.L. Tabarés et al., "Commissioning and first results of the OLMAT facility", submitted to Fusion Eng. Des.
[10] E. Oyarzabal, F.L. Tabarés, Deuterium retention of liquid Sn and SnLi in a CPS target under plasma exposure at high temperatures, Nucl. Fusion 61 (2021), 126033.
[11] E. de la Cal, et al., Two-dimensional imaging of edge plasma electron density and temperature by the passive helium emission ratio technique in TJ-II, Plasma Phys. Control. Fusion 53 (2011), 085006.